Journal of Hydrology: Regional Studies 33 (2021) 100768

Contents lists available at ScienceDirect

Journal of Hydrology: Regional Studies

journal homepage: www.elsevier.com/locate/ejrh

Evaluation of precipitation elasticity using precipitation data from ground and satellite-based estimates and watershed modeling in Western Nepal

Rocky Talchabhadel [a,*], Anil Aryal [b], Kenji Kawaike [c], Kazuki Yamanoi [c], Hajime Nakagawa [c], Binod Bhatta [d], Saroj Karki [e], Bhesh Raj Thapa [f]

[a] Texas A&M AgriLife Research, Texas A&M University, El Paso, USA
[b] Interdisciplinary Centre for River Basin Environment, University of Yamanashi, Japan
[c] Disaster Prevention Research Institute, Kyoto University, Japan
[d] Jade Consult Pvt. Ltd., Nepal
[e] Ministry of Physical Infrastructure Development, Province-1, Province Government, Nepal
[f] Universal Engineering and Science College, Nepal

ARTICLE INFO

Keywords:
Hydrologic model
Precipitation elasticity
Satellite-based precipitation estimate (SPE)
Soil and Water assessment Tool (SWAT)

ABSTRACT

Study Region: West Rapti River (WRR) basin, Western Nepal.
Study Focus: Hydrologic modeling requires an accurate precipitation data at a high spatial resolution, which is often limited in many regions of the globe. As a complement to the ground (gauge) precipitation data, satellite-based precipitation estimates (SPEs) appear useful. At first, this study evaluated performance of three different SPEs, namely i) CHIRPS, ii) PERSIANN-CCS, and iii) IMERG, with respect to gauge data using different event detection and quantification indices. Soil Water Assessment Tool (SWAT), a semi-distributed hydrologic model, was used to simulate the river discharge. We then analysed precipitation elasticity, as a first kind of such study in Nepalese river basin, by scaling the precipitation input in both positive and negative directions (ranging from -20 % to +20 %) in order to explore basin response on likely alteration of precipitation. A non-parametric precipitation elasticity was finally computed for three different cases: 1) observed river discharge, 2) gauge-based simulated river discharge, and 3) SPEs-based simulated river discharge.
New Hydrologic Insights for the Region: IMERG proved to be superior among three SPEs. All SPEs showed improved results after implementation of different levels of bias-correction where daily precipitation data were corrected using linear correction factors computed at a mean monthly scale. Computed correction factors are replicable to nearby basins. Precipitation elasticity of the study area ranged from +1.3 to +2.0 (approximately +1.5) which indicates that a 1.0 % change in precipitation will result in 1.5 % change in river discharge.

1. Introduction

Climate (precipitation, temperature, humidity, etc.) and anthropogenic (land use and land cover change, urban heat islands, etc.)

* Corresponding author at: 1380 A&M Circle, El Paso, TX, 79929, USA.
E-mail address: rocky.talchabhadel@ag.tamu.edu (R. Talchabhadel).

https://doi.org/10.1016/j.ejrh.2020.100768
Received 6 July 2020; Received in revised form 28 November 2020; Accepted 4 December 2020
Available online 17 December 2020

factors largely attribute to the hydrologic characteristics of a river basin (Xue et al., 2017; Zhang et al., 2016). And among several climatic variables, precipitation is one of the key components of the energy-water cycle (Kidd et al., 2017) which directly governs the basin hydrology. Reliable representation of the spatio-temporal variability of the catchment processes is a key challenge in hydrologic modeling (Dembélé et al., 2020). On the other hand, understanding of the sensitivity of river discharge to precipitation (i.e. simply precipitation elasticity) is vital for the effective management of water resources (Pandey et al., 2020b; Vano et al., 2012). To this end, characterization of a basin hydrology is often achieved through hydrologic models with precipitation being a major driving variable. Meanwhile, the application of hydrologic models for water resources assessment and management necessitates the adequately distributed precipitation information for reliable prediction (Cole and Moore, 2008; Sanchez-Moreno et al., 2014). But the use of hydrologic model to any river basin is often hindered due to the scantly available information on precipitation within a basin (Berg et al., 2016).

The precipitation information is generally derived from the ground-based rain gauges, meteorological radars, and satellite-based estimates. The accuracy of gauge data is usually greater in comparison to other estimates (Berg et al., 2016; Brocca et al., 2019). However, their spatial density is limited in many regions (Kidd et al., 2017) especially in developing countries like Nepal (Behrangi et al., 2011; Montanari et al., 2015; Thapa et al., 2016; Kumar et al., 2017; Maidment et al., 2017) which is further characterized by wide topographic variation (Alazzy et al., 2017), in particular ranging from over 8000 m to as low as 60 m above sea level (asl) across Nepal. In addition, such country either does not possess meteorological radars (or has installed recently) primarily due to economic and technological constraints. Under such a scenario, satellite-based precipitation estimates (SPEs) have the potential to overcome the limitations rendered by the low spatial density of ground-based rain-gauge stations (Bui et al., 2019; Dembélé et al., 2020; Siddique-E-Akbor et al., 2014). SPEs in general can complement the gauged data particularly where the observations are scarce (Tang et al., 2009).

With the advancement in satellite technology, different countries are successfully operating several missions for the observation of climatic variables (OECD, 2008). Furthermore, SPEs have been available across the globe for more than four decades now. The proliferation of satellite-based products in the recent times has given a greater access to different climatic data than ever before (Levizzani and Cattani, 2019; Sun et al., 2018). At the same time, the availability of such multiple SPEs may also likely puzzle the water-resources practitioners and decision-makers about the choice of any products. Therefore, the assessment of the accuracy and performances evaluation are prerequisites for any SPEs before using them for any water resources planning or decision-making (Maggioni et al., 2016; Wehbe et al., 2017). The use of multiple sensors for the estimation of precipitation has indicated promising results recently (Brocca et al., 2019). It is well understood that blending of satellite, station and reanalysis data could augment our understanding of the spatial characteristics of precipitation particularly in data scarce region (Beck et al., 2017; Ning et al., 2017). We need to understand that any SPEs might contain systematic and random biases. A performance test of SPEs is necessary before applying to any hydrologic models. In general, performances of SPEs are strongly location dependent.

In this context, this study used daily precipitation data of gauge and three SPEs: 1) Climate Hazards Group InfraRed Precipitation (CHIRP) with Stations (CHIRPS, 0.05° spatial resolution), 2) Precipitation Estimation from Remotely Sensed Information using Artificial Neural Networks - Cloud Classification System (PERSIANN-CCS, 0.04° spatial resolution), and 3) Integrated Multi-satellitE Retrievals for GPM (IMERG) - Final version (hereinafter IMERG, 0.1° spatial resolution). The selected three SPEs have higher spatial resolutions ($\leq 0.1^\circ \sim 10$ km) compared to other available products. Other promising products such as PERSIANN-Climate Data Record (PERSIANN-CDR), and Tropical Rainfall Measuring Mission (TRMM) Multi-Satellite Precipitation Analysis (TMPA), both available at 0,25° grid were not included in this study due to their coarser resolution.

Hydrologic models are regarded as one of the indispensable tools for better understanding the hydrologic characteristics of a basin which are imperative for making decisions on water resources management and planning (Singh, 2018). At the same time, the application of these models can also be crucial in performing various scenario and sensitivity analysis like land use or climate change impact analysis (Abbaspour et al., 2009; Dwarakish and Ganasri, 2015; Qiu et al., 2019). Due to high spatio-temporal variability of SPEs, drawing a prior conclusion on their accuracy is not straightforward, particularly when the corresponding observed data are limited (Zandler et al., 2019).

Among different hydrologic components, river discharge at a particular location could be of prime interest for the design of dams, hydropower projects, flood management or other water resources schemes (Johnston and Smakhtin, 2014; Masaki et al., 2017). In this regard, hydrologic model can be employed for predicting river discharge with different input SPEs and compared against the observed discharge for the performance evaluation (Tarek et al., 2020; Yang et al., 2014). Similar to the rain gauge stations, the number of hydrologic stations is highly limited and these stations may contain various sources of errors (Tarek et al., 2020). However, for this study we assumed the river discharge data are best available estimates. It is equally labor-, time- and cost-intensive for maintaining hydrologic stations at different river reaches. Therefore, hydrologic models are commonly used to simulate various hydrologic processes at different spatial scales.

Various hydrologic models are available depending on the nature, size and characteristics of the study area, objective of the research, and applications. Soil and Water Assessment Tool (SWAT) is chosen in this study mainly for its extended applicability to simulate long-term basin-scale hydrologic processes and perform different scenario analysis, among others. SWAT is one of the widely acknowledged hydrologic tools for watershed modeling as evident from Wang et al. (2019) who reported more than 3000 leading journal papers related to SWAT application globally (Science Citation Index Expanded, SCI-E) from 2008 to 2019 as retrieved on Jan 2019. Numerous SWAT related applications have been performed in different Nepalese river basins [by both national and international researchers] to simulate basin-scale hydrology, climate change impacts, land use change impacts etc. (Aryal et al., 2019; Bharati et al., 2016; Bhatta et al., 2019; Dahal et al., 2016; Mishra et al., 2018; Pandey et al., 2019; Thapa et al., 2017, 2016).

There are several adjacent watersheds that either do not possess any meteorological stations or have an insufficient number of

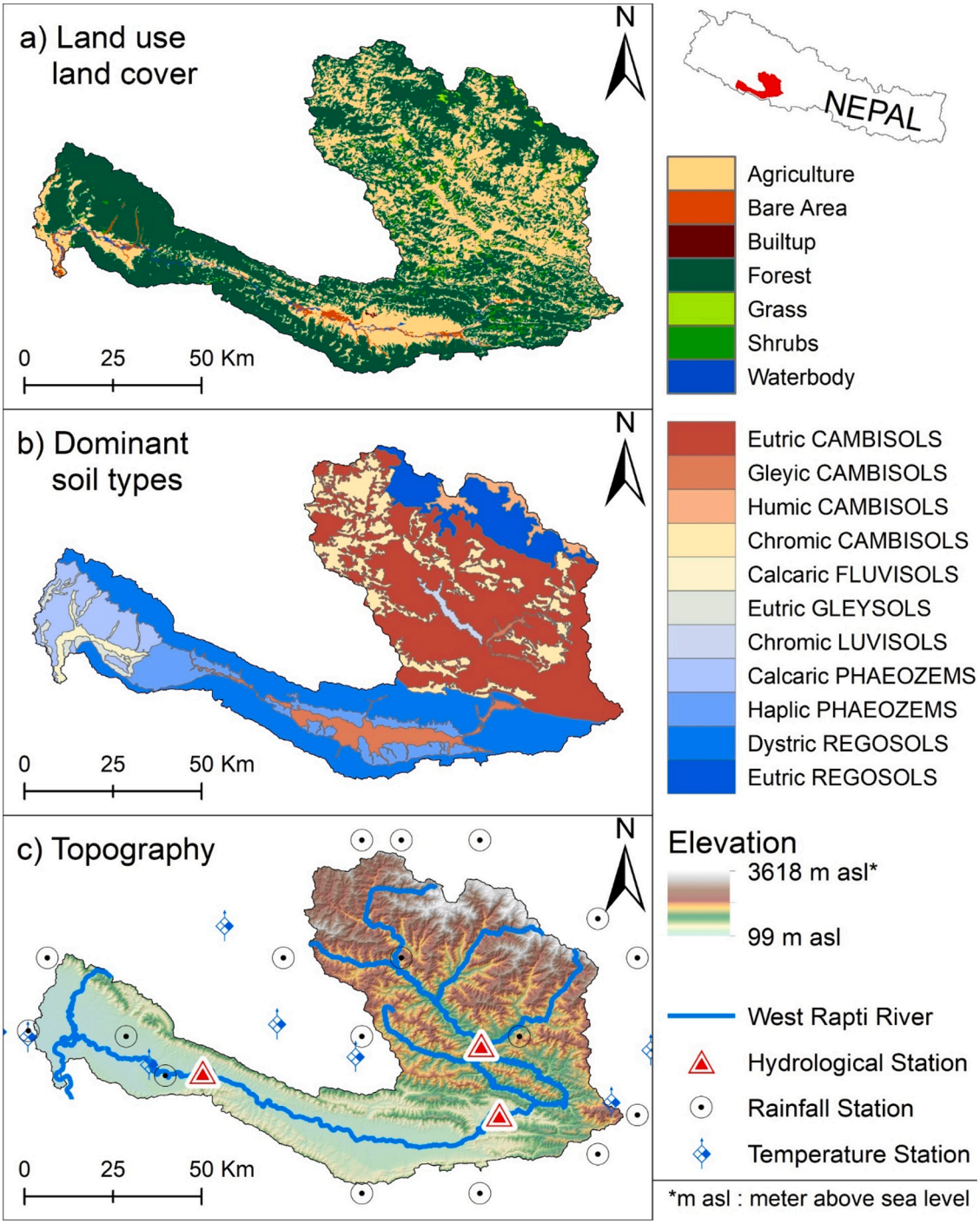

Fig. 1. a) Land use land cover, b) soil data, and c) topography of the West Rapti River basin. Network of hydro-meteorological stations is superimposed over the topography of the study area.

meteorological stations. Furthermore, such watersheds do not have long term river discharge data which hinders the planning of water-related schemes. The results of this study especially watershed parameters, and correction factors of SPEs could be transferred to adjacent watersheds to simulate hydrologic processes and evaluate precipitation elasticity based on different SPEs. A sound understanding of watershed response to precipitation is essential (Pandey et al., 2020b) for introducing any water resources-related developmental or disaster-mitigation plans including hydropower, irrigation or river-training works.

We selected West Rapti River (WRR) basin as the study area because of the availability of a comparatively denser network of hydro-

meteorological stations and as a representative of watersheds of western region of Nepal, which are quite less explored on. Nonetheless, we believe that the methodology adopted in this study can be applied even to any data-scarce watersheds or watershed having a sparse gauge network. The key objectives of this study are i) to assess the performance of SPEs, ii) to fed them in hydrologic model (SWAT) to simulate river discharge, and iii) to finally evaluate precipitation elasticity of the watershed using both ground and satellite-based precipitation data.

2. Materials and methods

2.1. Study area

WRR basin is located in the southern parts of western Nepal (shown in Fig. 1). Geographically, the study area extends from 27°40' to 28°35' North latitudes and 81°40' to 83°10' East longitudes. Fig. 1a) and b) show land use land cover (LULC) and soil data of the study area. The LULC map for the year 2010 adopted in this study was produced by the International Centre for Integrated Mountain Development (ICIMOD, 2013) at a spatial resolution of 30 m, and details on LULC data are available in Uddin et al. (2015). Agriculture and forest comprising 33 % and 60 % of the study area respectively are the two dominant land cover types in the basin (Talchabhadel et al., 2020b). The soil data was obtained from Soil and Terrain Database (SOTER), spatial resolution 1: 1,000,000. The topographical data used in this study is Advanced Space-borne Thermal Emission and Reflection Radiometer (ASTER) Global Digital Elevation Model Version GDEM version 3. The elevation ranges from about 100 m to over 3600 m asl within a small latitude extent (depicted in Fig. 1c). A network of hydro-meteorological station is presented in Fig. 1c.

The upper region of the study area is characterized by temperate climate whereas the lower regions experience a tropical climate (Karki et al., 2016). The length of main river channel from its origin to Indo-Nepal border is about 250 km. The precipitation is dominated by monsoonal system where approximately 80 % of annual precipitation occurs in monsoon period which extends through June to September (Talchabhadel et al., 2018). More precisely, July alone contributes about 28 % (ranging from 23 % to 32.4 % at different stations) of the annual precipitation. In contrast, November and December contribute less than 1% of the annual precipitation varying from 0.1 % to 1.2 % for November and 0.2%–1.7% for December at different stations(Talchabhadel et al., 2020a). Overall, the amount and the duration of direct runoff are meagre in non-monsoon period.

The WRR originates from the middle mountains of the country, enters the lowlands and finally drains to Ganges in India. It is joined by several tributaries like Jhimruk, Mari, Arun, Lungri, Sit, Danduwa, Sotiya, and Gadheli (Talchabhadel and Sharma, 2014). From the downstream of the confluence of Mari and Jhimruk rivers, the river is named the WRR. In this study, three hydrologic stations were used, namely Mari at upstream tributary (hereinafter upstream), Bagasoti after the confluence of upstream tributaries (hereinafter midstream), and Jakundi at downstream station (hereinafter downstream). The catchment areas at the upstream, midstream, and the downstream are 1980 km^2, 3380 km^2, and 5082 km^2 respectively.

2.2. Hydro-meteorological data

This study used daily precipitation data from 18 precipitation stations, temperature data from 8 climate stations and mean daily discharge (MDD) data from 3 hydrologic stations (locations are shown in Fig. 1c and meta data available in Table S1 in the supplement section) maintained by the Department of Hydrology and Meteorology (DHM), Government of Nepal (GoN) for the period of 1981−2015. Weather radar and satellite are the two other data sources that can provide a viable alternative to gauge data. Since weather radar is not available, this study attempts to assess the appraisal of SPEs. This study used three SPEs based on multiple satellite-based products: 1) CHIRPS (1981–2015), 2) PERSIANN-CCS (2003–2015), and 3) IMERG (2000–2015).

CHIRPS, available from 1981 onwards, is a quasi-global precipitation data set that blends satellite and gauge precipitation data. At first, infrared precipitation pentad (5-day) estimates are created from satellite data using information of cloud temperature and are calibrated with respect to (wrt) the TMPA pentads. These pentads are divided by its long-term (1981–2013) normal values and the fractions, multiplied against the corresponding Climate Hazards Precipitation (Funk et al., 2015b), provide CHIRP estimates. Finally, pentad CHIRP values are redistributed to daily precipitation estimates based on daily NOAA-CFS (National Oceanic and Atmospheric Administration - Climate Forecast System). CHIRP data is finally blended with stations data to generate CHIRPS product. Please follow (Funk et al., 2015a) for the detailed information of algorithm, CHIRPS station data merging.

Geostationary satellites are capable of providing images every 15−30 min in multiple spectral bands of the cloud patterns and evolution over time (Ashouri et al., 2015). PERSIANN system employs neural network methods to estimate precipitation using the information of the infrared brightness temperature image provided by these geostationary satellites. PERSIANN-CCS is a real-time global high-resolution satellite product that enables the categorization of cloud-patch features based on cloud height, areal extent, and variability of texture estimated from satellite imagery. The detailed description of PERSIANN family is discussed in Nguyen et al. (2018). PERSIANN-CCS data is available 2003 onwards. Thapa et al. (2016) used PERSIANN-CCS in mountainous regions of Bagmati River basin in Nepal to simulate the river discharge using the SWAT model.

IMERG estimates precipitation from the various passive microwave (PMW) sensors comprising the GPM (Global Precipitation Measurement) constellation. Precipitation estimates are computed employing Goddard Profiling Algorithm (GPROF2017). Please follow Huffman et al. (2019) for the detailed information. We used 06B version Final products of IMERG (herein after IMERG) which is available after ~ 3.5 months of observation time after the concluding calibration based on monthly GPCC (Global Precipitation Climatology Centre) gauge-based dataset. Table 1 shows a summary of data used in this study.

Table 1
Data type, properties and sources used in this study.

Dataset (unit)	Data type (resolution)	Source	Time frame, remarks
Topography (m)	Spatial grids (30 m)	ASTER GDEM v3	2000–2013, published on 2019
Land use land cover, LULC	Spatial grids (30 m)	ICIMOD	2010, based on Landsat TM images
Soil type	Spatial vector (based on 1: 1 million scale)	SOTER	1980−1990, published on 2009
Temperature (^{o}C)	Time series (daily)	DHM	1981−2015, 7 stations
Precipitation (mm)	Time series (daily)	DHM	1981−2015, 18 stations
SPEs (mm)	Spatial grids (4 km), Time series (daily)	PERSIANN-CCS	2003−2015
	Spatial grids (5 km), Time series (daily)	CHIRPS	1981−2015
	Spatial grids (10 km), Time series (daily)	IMERG Final	2000−2015
Mean daily discharge (m^3/s)	Time series (daily)	DHM	1981−2015, 3 stations

ASTER: Advanced Spaceborne Thermal Emission and Reflection Radiometer; GDEM: Global Digital Elevation Model Version.
ICIMOD: International Centre for Integrated Mountain Development; TM: Thematic Mapper.
SOTER: Soil and Terrain Database; DHM: Department of Hydrology and Meteorology; SPEs: Satellite-based precipitation estimates.
PERSIANN-CCS: Precipitation Estimation from Remotely Sensed Information using Artificial Neural Networks-Cloud Classification System.
CHIRPS: Climate Hazards Group InfraRed Precipitation with Stations.
IMERG: Integrated Multi-satellitE Retrievals for GPM; GPM: Global Precipitation Measurement.

Table 2
Indices for precipitation event detection evaluation.

Detection status		SPEs	Gauge
True	T	Rain	Rain
False	F	Rain	No rain
Miss	M	No rain	Rain
Null	X	No rain	No rain

Detection indices		Equation	Range	Ideal Value
Probability of Detection	POD	T/(T + M)	0 to 1	1
Critical Success Index	CSI	T/(T + M+F)	0 to 1	1
False Alarm Ratio	FAR	F/(T + F)	0 to 1	0
Frequency Bias Index	FBI	(T + F)/(T + M)	0 to ∞	1

Threshold for rain = 1 mm/day.
SPEs: Satellite-based precipitation estimates.

2.3. Evaluation of satellite-based precipitation estimates

Inter-comparisons of different SPEs with daily gauge data were conducted at 18 precipitation stations for the aforementioned time period. This study employed 4 precipitation event detection indices: 1) probability of detection (POD), 2) critical success index (CSI), 3) false alarm ratio (FAR), and 4) frequency bias index (FBI). The calculation procedure is shown in Table 2.

POD, CSI, and FAR range from 0 to 1. A higher value represents an ideal condition for POD and CSI whereas lower value represents the ideal condition for FAR. The ideal value of FBI is 1. FBI ranges from 0 to ∞. POD indicates the proportion of correctly detected precipitation events to the total number of gauge-based precipitation events. Similarly, CSI indicates an overall proportion of correctly detected precipitation events to the total number of precipitation events either detected by satellite or gauge. In contrast, FBI denotes the proportion of false status to the total number of precipitation events detected by satellite. FBI represents a simple bias between satellite detected precipitation events to the gauge-based precipitation events. FBI values >1 represents over estimation of precipitation event detection and <1 represent under estimation of precipitation event detection.

We computed quantitative evaluation of different SPEs using root mean square error (RMSE), and percentage bias (PBIAS) wrt gauge data.

$$RMSE = \sqrt{\frac{1}{N}\sum\left(SPE_i - Gauge_i\right)^2} \tag{1}$$

$$PBIAS = \frac{\sum\left(SPE_i - Gauge_i\right)}{\sum Gauge_i} \times 100 \tag{2}$$

Here, negative value of PBIAS represents underestimation, positive value represents overestimation, and perfect zero represents ideal (i.e. without any volume bias) for SPEs wrt gauge data. A lower value is best for RMSE.

A linear scaling method of bias-correction was used to correct biases of SPEs. Monthly correction factors ($CF = Gauge/SPEs$) were computed by comparing basin averaged precipitation based on gauge and SPEs on a mean monthly scale. Computed monthly correction factors were then multiplied to the raw daily precipitation data at every station on corresponding months. It is to be taken care that if the data quality of gauge precipitation data is poor, it might lead to unrealistic representation of SPEs. In particular, there

are high chances of low data quality in remote stations across the mountainous terrain. In case of selected study area, there were negligible data gaps and the selected study area is one of the basins of Nepal having high quality observed data. The computed correction factors could be transferred to nearby ungauged basins.

2.4. SWAT model

SWAT model is a continuous-time, semi-distributed, physically-based, river basin-scale model operated at daily or hourly time steps. The model has widely been applied to different river basins, gauged or ungauged, across the globe. Major model components include weather, hydrology, soil, plant growth, sediments/nutrients, and land management (Arnold et al., 2012b). All the equations incorporated in the model are described in the very comprehensive theoretical documentation manual (Neitsch et al., 2011). Among different available SWAT modules and resources like QSWAT, SWAT/GRASS, and different modified SWAT models, ArcSWAT (Olivera et al., 2006) is one of the popular and user friendly modules for setting up the model, and modifying input parameters. The watershed modeling in this study is based on ArcSWAT 2012.

In SWAT, a watershed is discretized into multiple sub-basins. Each sub-basin is further divided into multiple hydrologic response units (HRUs), smallest units consisting of homogenous soil characteristics, land use, and topographical settings (Neitsch et al., 2011). In this study, WRR basin was delineated into 30 sub-basins which was further divided into 488 HRUs. Runoff from all HRUs within a sub-basin are summed and enter the main reach of the sub-basin and they are routed through the channel network to the outlet of the watershed. The water balance expression used in the SWAT model is:

$$SW_t = SW_0 + \sum_{i=1}^{t}\left(R_{day} - Q_{surf} - E_a - W_{seep} - Q_{gw}\right) \quad (5)$$

where SW_t and SW_0 are the final and early stage water contents of the soil respectively, t is time in days, R_{day} is the daily precipitation, Q_{surf} is the daily surface runoff, E_a is the daily evapotranspiration, W_{seep} is the daily percolation, and Q_{gw} is the daily return flow, all units are in mm.

Surface runoff is most commonly simulated using the SCS curve number (SCS-CN) method in the SWAT. The SCS-CN method is a rainfall-runoff model that computes excess runoff (King et al., 1999) which assumes an initial abstraction could be defined as a percentage of potential maximum retention after runoff begins, that is related to the curve number (Neitsch et al., 2011).

2.5. SWAT calibration and validation

Accurate calibration of any hydrologic models (including SWAT) followed by the validation is a routine yet a key step during the water balance, flood or similar hydrologic modeling. SWAT being a physically-based model requires the input parameters be held within a realistic uncertainty range. Sensitivity analysis, which determines the most sensitive parameters of the basin, precedes the model calibration and validation processes. This study employed a global sensitivity analysis, by allowing all parameter values to change (Arnold et al., 2012b). Once the sensitive parameters are identified, model calibration is performed next. Model calibration involves a careful allocation of values for the selected input parameters (within their respective uncertainty range) such that model estimations (simulated output) and observed (gauge) data are in a close agreement with each other. Finally, in the validation step, the model is simulated for a separate time period not included in the calibration keeping the same parameters obtained from the calibration.

In this study, the period of five years from 1981 to 1985 was considered as the warm-up period while 1986–2005 (20 years), and 2006–2015 (10 years) were used as the calibration and validation periods respectively for the river discharge. This study used gauge precipitation data for calibration/validation process and later forced different SPEs to the calibrated model. To represent the spatial heterogeneity of the basin, three discharge gauging stations (namely Mari at upstream, Bagasoti at midstream, and Jalkundi at downstream) were used for multi-site calibration and validation process. A Sequential Uncertainty Fitting (SUFI-2) (Abbaspour et al., 2004), a semi-automated approach, was employed using the SWAT-CUP (SWAT – Calibration Uncertainty Procedure). SWAT-CUP is the most widely used tool for performing parameterization, sensitivity and uncertainty analysis, calibration, and validation of input parameters.

500 simulations were performed in first iteration for fine-tuning of 36 selected input parameters (shown in Table S2 in supplement section). The parameters were selected by referring literatures (Arnold et al., 2012a) and published studies (Dhami et al., 2018; Bhatta et al., 2019; Pandey et al., 2019, 2020) across Nepal. Finally, two iterations of 500 simulations each, meaning 1000 simulations, were performed with revised ranges of most sensitive parameters ($p \leq 0.1$) for the study area. Nash-Sutcliffe efficiency, NSE (Nash and Sutcliffe, 1970) was chosen as an objective function because of its wide application. NSE is a normalized index that tells the magnitude of residual variance, compared to observed variance. In addition, percentage bias (PBIAS), and coefficient of determination (R^2) between simulated and observed river discharge were also checked. Please see Krause et al. (2005) and Moriasi et al. (2007) for a detailed information on these indices. Here, negative values of PBIAS represent underestimation and positive values represent overestimation of simulate river discharge wrt observed ones. We also performed manual calibration of few parameters related to baseflow after auto-calibration based on knowledge of the basin. Finally, the calibrated and validated model was then fed with raw and bias-corrected SPEs.

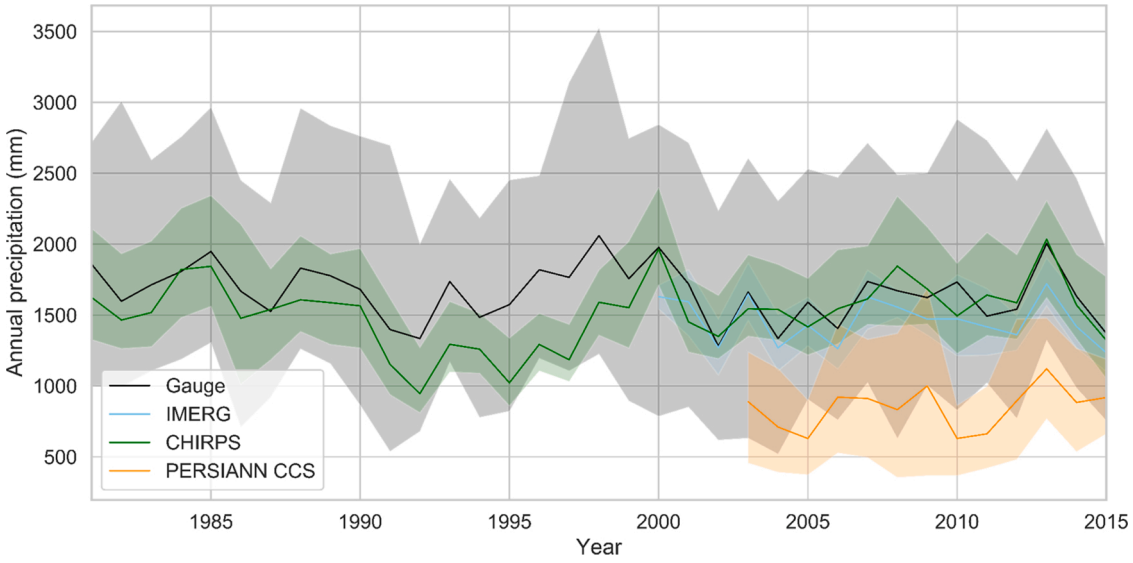

Fig. 2. Temporal variation of annual precipitation based on gauge and satellite-based precipitation estimates (SPEs) data for the period of 1981 – 2015 in the West Rapti River basin. Spread represents the range of annual precipitation from the lowest to the highest for all stations distributed across the study area.

2.6. Precipitation elasticity estimation

The sensitivity of the total river discharge estimated by SWAT to the precipitation was evaluated by: scaling the gauge precipitation data; running the calibrated model; and then comparing with simulated river discharge using the original data. The daily precipitation time series was scaled by -20 %, -10 %, +10 % and +20 %. The precipitation elasticity of river discharge was evaluated using following expression:

$$\Delta Q = \varepsilon_p \Delta P \tag{6}$$

where, ΔQ is change in simulated mean annual river discharge, and ΔP is change in annual rainfall, and ε_p is precipitation elasticity of river discharge. Apart from simulation there exists other different methods to estimate precipitation elasticity. Pandey et al. (2020b) assessed climate elasticity including precipitation elasticity using different methods based on water balance models for an extended East Rapti watershed, adjacent to current study area. In this study we used a simple and popular non-parametric estimator, Sankarasubramanian et al. (2001)'s approach, to estimate precipitation elasticity of river discharge which is the proportional change in river discharge divided by the proportional change in precipitation. It can be expressed as:

$$\varepsilon_p{}^{NP} = median\left(\frac{\left(Q_i - \overline{Q}\right)\overline{P}}{\left(P_i - \overline{P}\right)\overline{Q}}\right) \tag{7}$$

where, $\varepsilon_p{}^{NP}$ is the precipitation elasticity of river discharge based on the non-parametric estimator, $\overline{P}$ and $\overline{Q}$ are mean annual precipitation and river discharge respectively for the study period, P_i and Q_i are annual precipitation and river discharge respectively for the i^{th} year. Precipitation elasticity of river discharge provides a measure of the sensitivity of river discharge to precipitation. A value >1 indicates that a 1% change in precipitation can cause >1% change in river discharge. In this study, $\varepsilon_p{}^{NP}$ was determined for three different cases: 1) observed river discharge, 2) gauge-based simulated river discharge, and 3) SPEs-based simulated discharge. This method has a numerical problem when P_i approaches $\overline{P}$ causing ε_p tends to ∞ for that i^{th} year.

3. Results and discussions

3.1. Evaluation of selected precipitation products

Most of the stations cover a complete span of length except a few stations (407 Kusum, 502 Shera Gaun, 515 Ghorai, and 631 Bhing githe). It should be noted that the (515) Ghorai and the (631) Bhin githe are new weather stations installed recently (Talchabhadel et al., 2020b). There are some stations where data were missing for few days in a year. The data gaps for the missing period were filled using information from the nearest spatial locations. Data gaps were significant in the year 2003, 2009, 2010, and 2013. Fig. 2 illustrates the temporal variation of annual precipitation derived from the gauge and three SPEs data for the study period. Spreads of all three SPEs, in particular IMERG and CHIRPS, are narrower compared to the spread of gauge data. Though these SPEs have high spatial

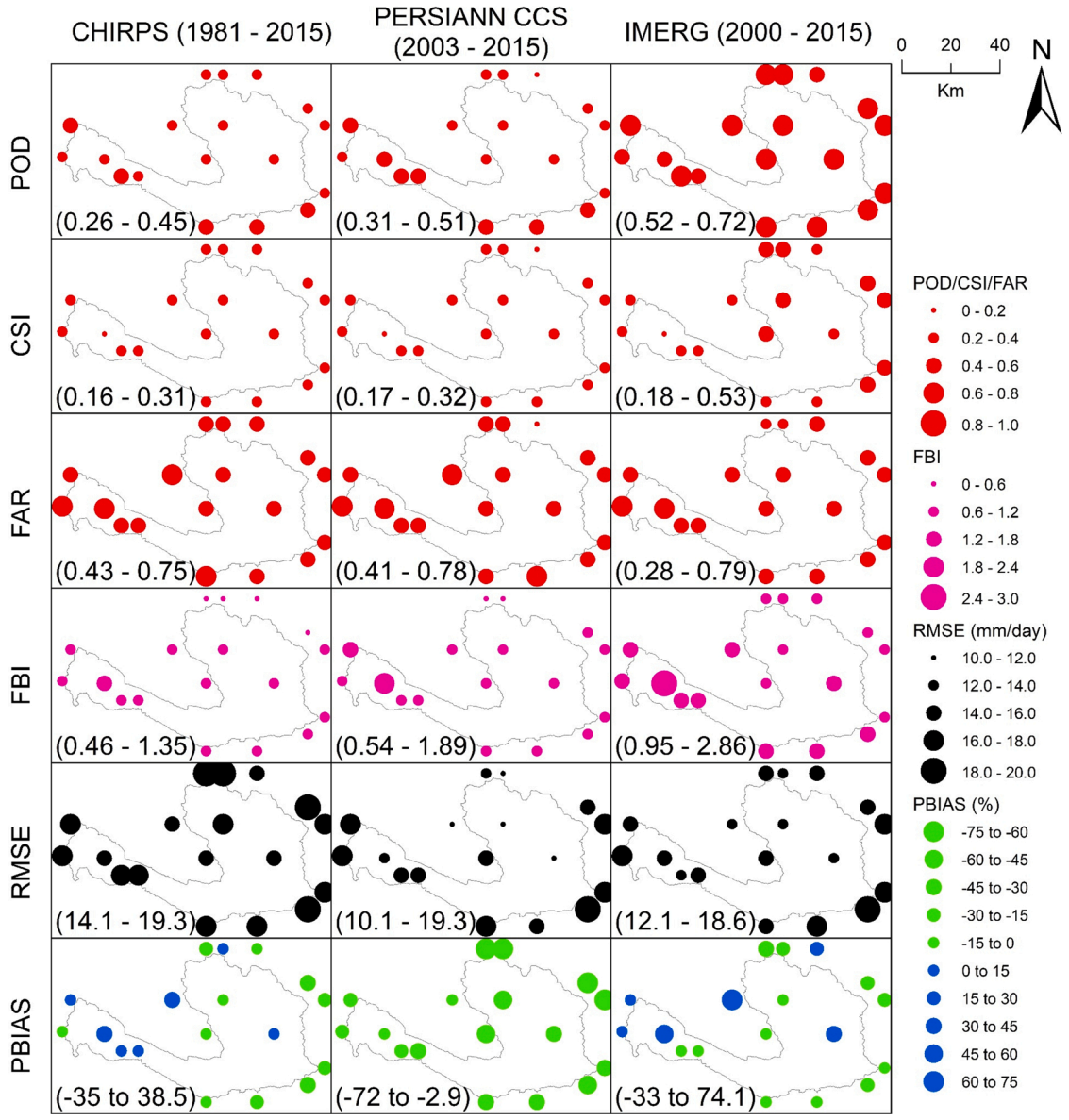

Fig. 3. Performance of different satellite-based precipitation estimates (SPEs) with respect to gauge data at stations across the study area. Values in parentheses represent the range of corresponding detection indices.

resolution ($\leq$10 km), these products are generally calibrated using coarse spatial resolution products ($\geq$ 25 km), spatial variations may not be well captured across hilly topography. More detailed comparative analysis considering the dependency on the elevation factor might be required for further rectification. This study attempts to evaluate the applicability of using these SPEs employing simple technique for hydrologic assessment.

We found that PERSIANN-CCS values were almost half of the gauge data. In general, CHIRPS and IMERG showed a similar pattern with gauge data. However, noticeable fluctuations were visible, for instance, CHIRPS during 90 s. During the 90 s, CHIRPS data indicated significantly reduced values of precipitation. However, before and after 90 s, CHIRPS data were largely congruous with the gauge data. Importantly, the tendency of inter annual variability is well captured by all three SPEs indicating a proper systematic bias could be detected and the bias could be reduced.

Fig. 3 depicts performance of different SPEs according to detection-based indices (POD, CSI, FAR, and FBI) and magnitude-based indices (RMSE, and PBIAS). CHIRPS and PERSIANN-CCS revealed lower POD values compared to IMERG. However, PERSIANN-CCS was found to be slightly better than CHIRPS in terms of POD. A similar pattern is observed for CSI values. In general, all SPEs showed noteworthy false alarms. The FAR values ranged from ~0.4 to ~0.8 for CHIRPS and PERSIANN-CCS and from ~0.3 to ~0.8 for IMERG. IMERG performed slightly better than the remaining two SPEs in terms of FAR. FBI values are almost similar for all three cases,

Table 3
Sensitive parameters ($p \leq 0.1$) out of 36 parameters used to calibrate and validate the model at three stations in the West Rapti River basin, using SUFI-2 in SWAT-CUP.

Rank	Parameter Name	Description (unit)	P-Value	lower bound	upper bound	fitted value
1	ALPHA_BNK	Baseflow alpha factor for bank storage (days)	0.00	0	0.6	0.2
2	LAT_TTIME	Lateral flow travel time (days)	0.00	0	105	28.1
3	CN2*	Initial SCS runoff curve number for moisture condition II	0.00	35	98	varies
4	CANMX	Maximum canopy storage (mm)	0.00	0	100	82
5	CH_K2	Effective hydraulic conductivity in main channel (mm/hr)	0.00	0	320	132
6	GWQMN	Threshold water level in shallow aquifer for baseflow (mm)	0.00	0	1700	900
7	SOL_Z*	Depth from soil surface to bottom of layer (mm)	0.00	0	3500	varies
8	RCHRG_DP	Deep aquifer percolation fraction	0.00	0	1	0.4
9	REVAPMN	Threshold water level in shallow aquifer for revap (mm)	0.00	0	200	91
10	GW_REVAP	Groundwater revap coefficient	0.01	0.06	0.19	0.1
11	SOL_AWC	Available water capacity (mm water/ mm soil)	0.01	0	1	0.28
12	CH_N2	Manning's roughness value for the main channel	0.03	0	0.3	0.11
13	CH_K1	Effective hydraulic conductivity in tributary channel (mm/hr)	0.04	0	300	230
14	SURLAG	Surface runoff lag coefficient	0.08	0	10	1.7
15	EPCO	Plant uptake compensation factor	0.10	0	1	0.81

the existing parameter is replaced by a new value.
* relative, the existing parameter is multiplied by (1 + a given value).

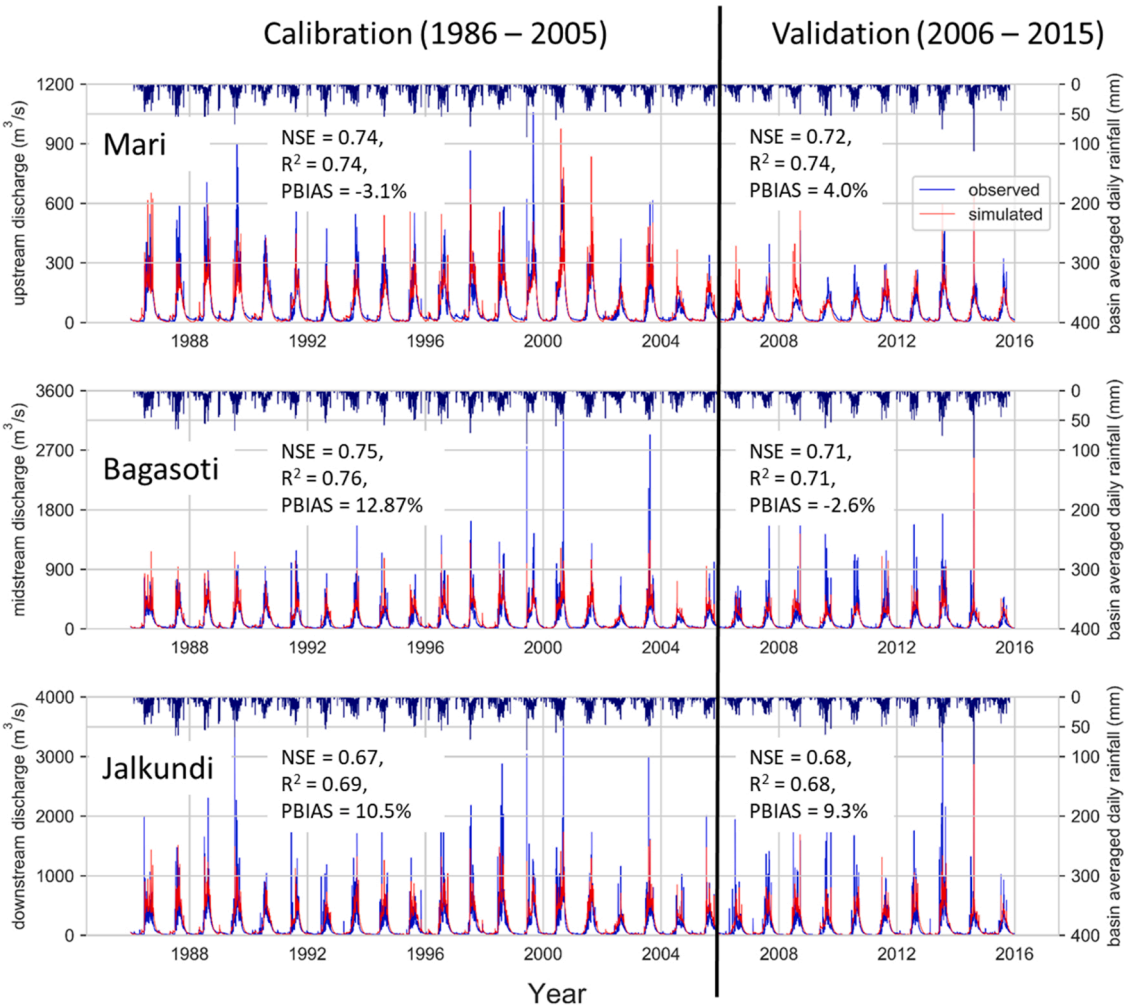

Fig. 4. Model performance at three hydrologic stations at upstream (Mari), midstream (Bagasoti) and downstream (Jalkundi) of the West Rapti River basin during calibration (1986 – 2005) and validation (2006 – 2015) periods. Basin averaged precipitation is computed using the stations located upstream of the hydrologic station and is shown facing downward for all three subplots accordingly.

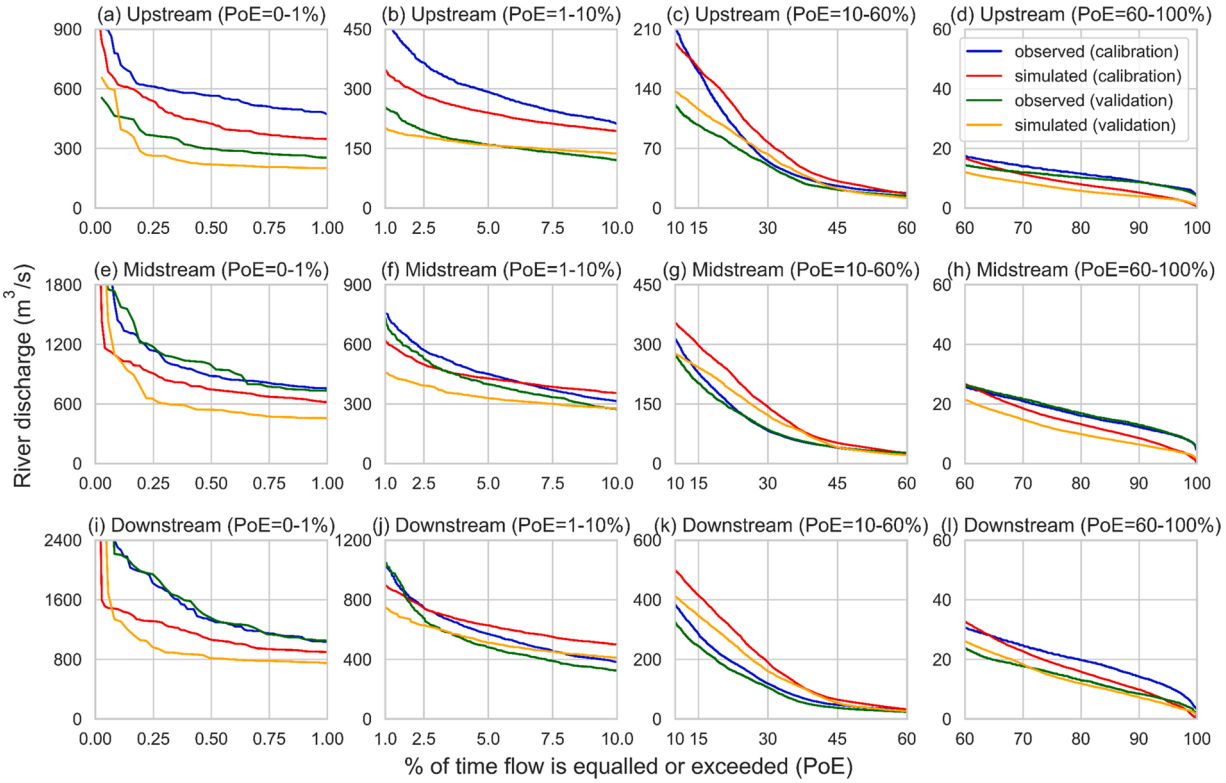

Fig. 5. Flow duration curve showing probability of exceedence (PoE) based on observed and simulated river discharge for calibration (1986-2005) and validation (2006-2015) periods based at three hydrologic stations (upstream a-d, midstream e-h, and downstream i-l) in West Rapti River basin. First, second, third and fourth columns from left represent PoE ranging 0-1% (extremely high flow), 1-10 % (high flow), 10 – 60 % (average flow), and 60-100 % (low flow) respectively.

however, IMERG showed a greater number of stations revealing overestimations of detections of precipitation whereas PERSIANN-CCS showed greater number of stations revealing underestimation of detections of precipitation.

PERSIANN-CCS clearly revealed substantial underestimated magnitudes in all stations across the study area. In contrast, CHIRPS and IMERG displayed a mixed pattern of under- and over-estimated magnitudes at different stations across the study area. But when we closely look into RMSE, the RMSE values ranged from 10 to 20 mm/day for all selected SPEs indicating that all three SPEs have positive or negative daily biases. Overall, based on detection- and magnitude- based indices, IMERG showed comparatively better performance. The subsequent sections offer discussion on results after feeding the raw and corrected SPEs and gauge data into hydrologic model.

3.2. *Performance of SWAT model*

We calibrated and validated the SWAT model at three hydrologic stations (at upstream, midstream and downstream). Table 3 shows the most sensitive parameters ($p \leq 0.1$) out of 36 selected parameters (shown in Table S2 in the supplement section). ALPHA_BNK, LAT_TTIME and CN2 were among the most sensitive parameters in the study area. A few parameters which are meaningfully sensitive to the river discharge including baseflow are ALPHA_BNK, SOL_AWC, and CANMX. ALPHA_BNK, baseflow alpha factor for bank storage (in days), characterizes the bank storage recession curve. Most of the sensitive parameters are congruent with other SWAT models (Bhatta et al., 2020; Dhami et al., 2018; Pandey et al., 2020a) calibrated across western Nepal. Higher the ALPHA_BNK values flatter the recession. LAT_TIME, lateral flow travel time (in days), describes the lateral flow in the basin and CN2, initial SCS curve number for moisture condition II, is a function of the soil's permeability, land use and antecedent soil water conditions. New sets of lower and upper bound for different parameters were set after sensitivity analysis and after another 1000 simulation runs, the best simulation was selected.

Fig. 4 shows the model performance during both the calibration and validation periods at three hydrologic stations at upstream, midstream, and downstream of the study area on a daily scale. Overall the values are acceptable (Moriasi et al., 2007) for a daily simulation. NSE and R^2 values ≥ 0.7 were observed during calibration and validation period in upstream and midstream locations and these values ~0.7 were observed at the downstream. PBIAS ~10 % at downstream in both calibration and validation periods indicates an overestimation at the downstream location of the study area. The PBIAS values at upstream and midstream stations are comparatively better. Our results indicated that the parameters in lower sub-basins and HRUs might need a further fine-tuning if specific analyses are desired in lower regions of the study area. Excluding some extremes (high and low flows), the model reproduced the river

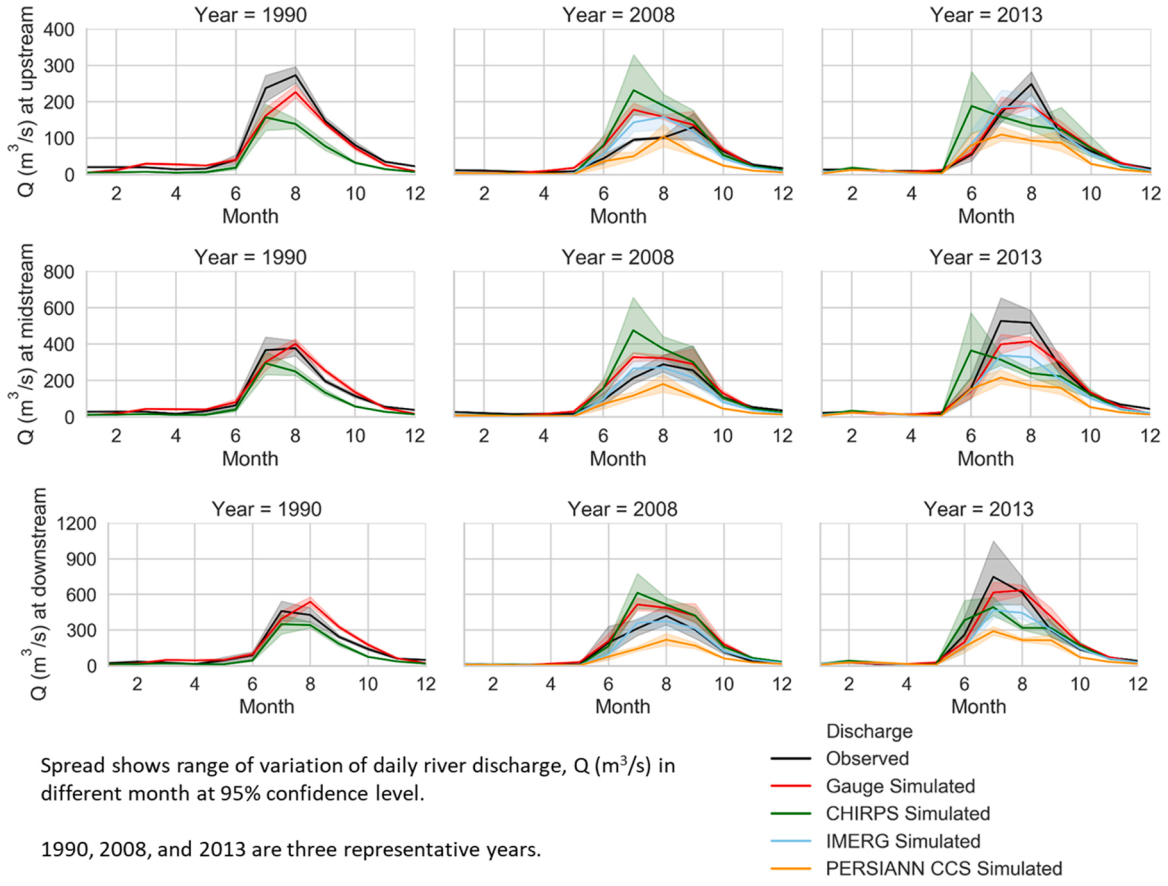

Fig. 6. Monthly variation of observed and simulated river discharge for different representative years based on gauge data and different satellite-based precipitation estimates (SPEs) at three hydrologic stations in West Rapti River basin.

discharge in an acceptable range throughout the simulation period from 1986 to 2015.

The probability of exceedance (PoE) informs the percentage of the time the flow is equalled or exceeded. The PoE for extremely high flow is very small as it is obvious that such an extreme discharge occurs for only a few numbers of time in a year. And for some cases, the return period might even cross > 50 or 100 years. In general, the SWAT model currently has a limitation to simulate such extreme cases (Bhatta et al., 2020; Dhami et al., 2018; Pandey et al., 2019, 2020). In addition, a continuous time marching in SWAT, limits its application for detailed, event-based flood simulation (Bhatta et al., 2020). For the analyses of different zones of river discharges based on PoEs, we categorized the river discharge into four ranges i) extremely high (PoE = 0–1%), ii) high (PoE = 1–10%), iii) average (PoE = 10–60 %), and iv) low (PoE = 60–100%).

Fig. 5 exhibits flow duration curve (FDC) at four different ranges based on PoE for the calibration and the validation period at three stations at upstream, midstream, and downstream of the study area. For the extremely high flow, the simulated discharge showed substantial underestimation which indicates that the SWAT model could not mimic the timing, intensity, and magnitude of peak flood (PoE ≤1%). Similar results were also reported by the previous studies (Dhami et al., 2018; Pandey et al., 2020a, 2019). For the high flow range, the model underestimated at the upstream station. However, the model began to overestimate in midstream and downstream locations at PoE ~ 5–10 %. For the average flow, the simulated discharge showed a slight overestimation whereas low flows were underestimated.

Low flows with PoE > 80 % are vital for water resources projects relying on dependable low flows like water supply, irrigation, agriculture and other environmental projects during dry periods while PoE<10 % (i.e. high flows) are crucial for flood disaster management. For a specific focus on these extremes, a careful selection of parameters, their sensitivity analyses, appropriate calibration/validation, and accordingly coupling with specific models are suggested. For instance, the SWAT model could be coupled with groundwater model for low flow analysis (Ahn et al., 2018) or with hydraulic models for high flow analysis (Schmalz et al., 2012).

Based on the above-mentioned reliability the current model is acceptable for a water balance analysis and could be used for any intervention analysis. Most of the water resources projects rely on the water at average flow, for instance, run off river (RoR) hydropower projects rely on PoE = 30–50 %. The model was then fed with different SPEs. Fig. 6 shows the monthly variation of river discharge for different representative years based on observed and simulated data (fed with gauge and different SPEs data). CHIRPS-simulated discharge occasionally showed peak value during the month of June whereas simulated and observed discharge showed the

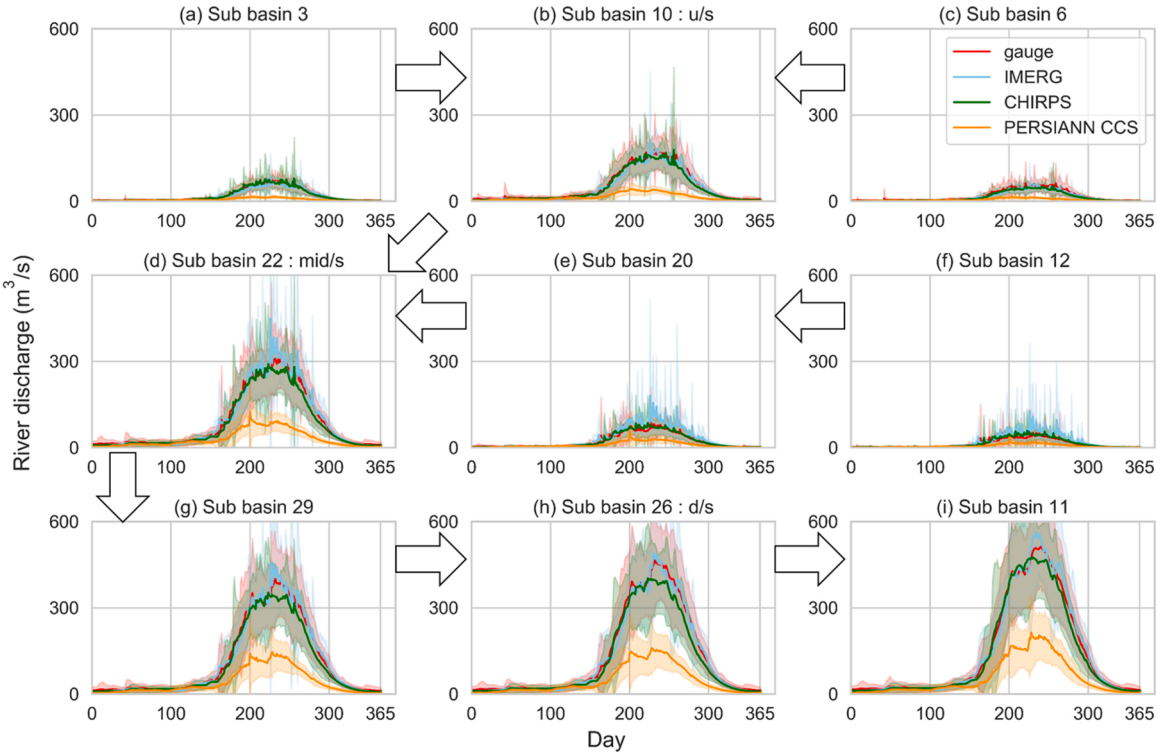

Fig. 7. Intra-annual variation of simulated river discharge based on gauged data and different satellite-based precipitation estimates (SPEs) at different reaches in West Rapti River basin. Subbasins 10, 22 and 26 are gauged stations namely upstream (u/s), midstream (m/s) and downstream (d/s) stations respectively. The arrow between two subbasins represents the river is flowing from subbasin at arrow tail to the subbasin at arrow head. Spread represents range of standard deviation of inter-annual variation of daily discharge.

Table 4
Mean monthly precipitation and monthly correction factors for different satellite-based precipitation estimates (SPEs) to correct daily precipitation data in the study area.

	Precipitation (mm/month)				Correction factor = Gauge/SPEs		
Month	Gauge	CHIRPS	IMERG	PERSIANN-CCS	CHIRPS	IMERG	PERSIANN-CCS
Jan	69.3	60.5	57.4	42.3	1.1	1.2	1.6
Feb	66.2	55.9	55.2	40.9	1.2	1.2	1.6
Mar	64.5	60.1	60.3	43.5	1.1	1.1	1.5
Apr	71.5	75.3	70.3	58.1	0.9	1.0	1.2
May	103.0	97.6	88.4	48.3	1.1	1.2	2.1
Jun	240.8	232.1	193.1	110.2	1.0	1.2	2.2
Jul	338.2	315.4	306.0	161.2	1.1	1.1	2.1
Aug	313.0	269.5	295.0	168.4	1.2	1.1	1.9
Sep	172.5	145.4	164.0	63.7	1.2	1.1	2.7
Oct	80.8	78.2	64.3	37.3	1.0	1.3	2.2
Nov	66.5	71.2	50.0	36.2	0.9	1.3	1.8
Dec	76.8	66.3	57.0	36.7	1.2	1.3	2.1

peak during either July or August. Figures S1, S2, and S3 in supplement section are for all years at upstream, midstream, and downstream stations, respectively. Most of the year, the tendency of intra-annual variability is well captured by all SPEs. In general, PERSIANN-CCS showed underestimated river discharge predominantly due to significant underestimated precipitation input wrt gauge data. The underestimation of CHIRPS precipitation during 90 s wrt gauge data resulted in a noticeable underestimation (though expected) of the river discharge. Overall, IMERG demonstrated an improved congruity with gauge simulated and observed river discharge most of the time.

Fig. 7 shows intra-annual variation of simulated river discharge based on gauged and different SPEs data at different representative sub-basins including three hydrologic stations. Use of hydrologic model allows us to explore how different sub-basins (from upstream to downstream) responded to different precipitation data sets and propagated. The most downstream sub-basin presents river discharge at Nepal-India border. Though the location is ungauged, calibrated hydrologic model informs likely river discharge during

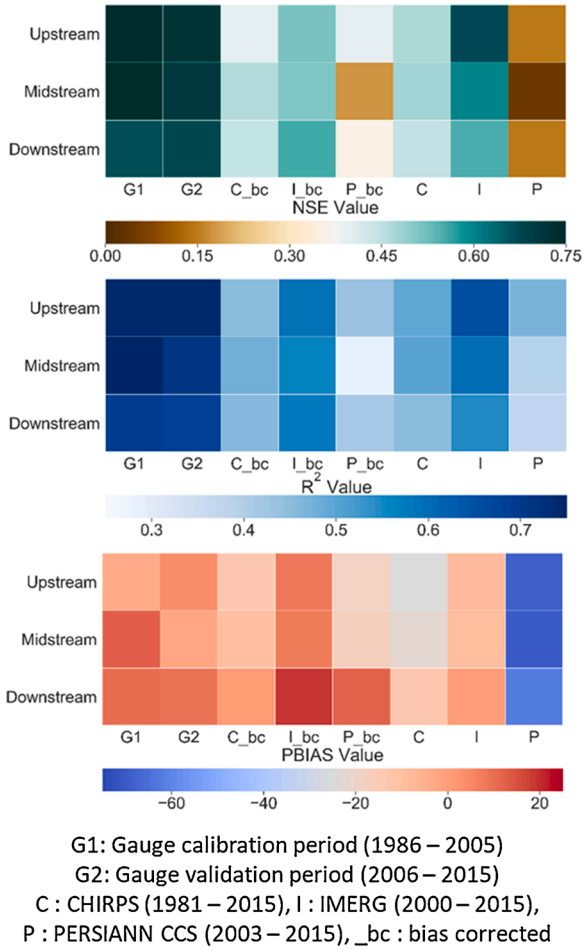

Fig. 8. SWAT Model performance based on NSE, R^2, and PBIAS values for the simulations based on gauge (calibration and validation periods), different satellite-based precipitation estimates (SPEs) in both raw and corrected forms at three stations in upstream, midstream and downstream of the study area.

different time periods. By forcing the model, different interventions could be simulated. At all selected sub-basins, IMERG and CHIRPS showed similar response as that of gauge data. In the case of PERSIANN-CCS, though the tendency is similar the magnitude is smaller. We applied a linear scaling of bias-correction to reduce the biases of different SPEs.

3.3. Bias-correction of SPEs and their application

For a specific study, correction factors could be determined on a daily, monthly, or annual scale, at every station or at a spatially averaged case. For the spatially varying correction factors, the correction factors would be local and their application to adjacent watershed demands site-specific gauge data. The rationale behind our study is not only to apply the correction factors for the selected catchment with a better precision but to apply the methodology and correction factors to either any data-scarce adjacent watersheds or the study area with similar catchment properties.

Table 4 shows mean monthly precipitation and monthly correction factors for different SPEs to correct the daily precipitation data in the study area. The mean monthly correction factors ranged from 0.9 to 1.2 for CHIRPS, 1.0–1.3 for IMERG and 1.5–2.7 for PERSIANN-CCS. For CHIRPS and IMERG, comparatively higher correction factors were observed during the non-monsoon period. In contrast, higher correction factors were observed during monsoon period for PERSIANN-CCS.

Table S3 in the supplement section shows station wise mean annual precipitation and the annual correction factor for different SPEs in the study area. The annual correction factor for CHIRPS and IMERG was found to be 1.1 while it was 1.9 for PERSIANN-CCS. Figure S4 in the supplement section shows intra-annual variations at different sub-basins similar to Fig. 7 but for bias-corrected SPEs. After introducing bias-correction at different levels, all SPEs showed improved results and they were nearly congruous with gauge-based simulation. These evidence support the implementation of bias-correction, though simple and spatially uniform. However, the use of PERSIANN-CCS should be limited when other products do much better job with lower level of bias-correction.

Fig. 8 shows performance evaluation of SWAT model based on NSE, R^2 and PBIAS values for the simulations; i) based on gauge

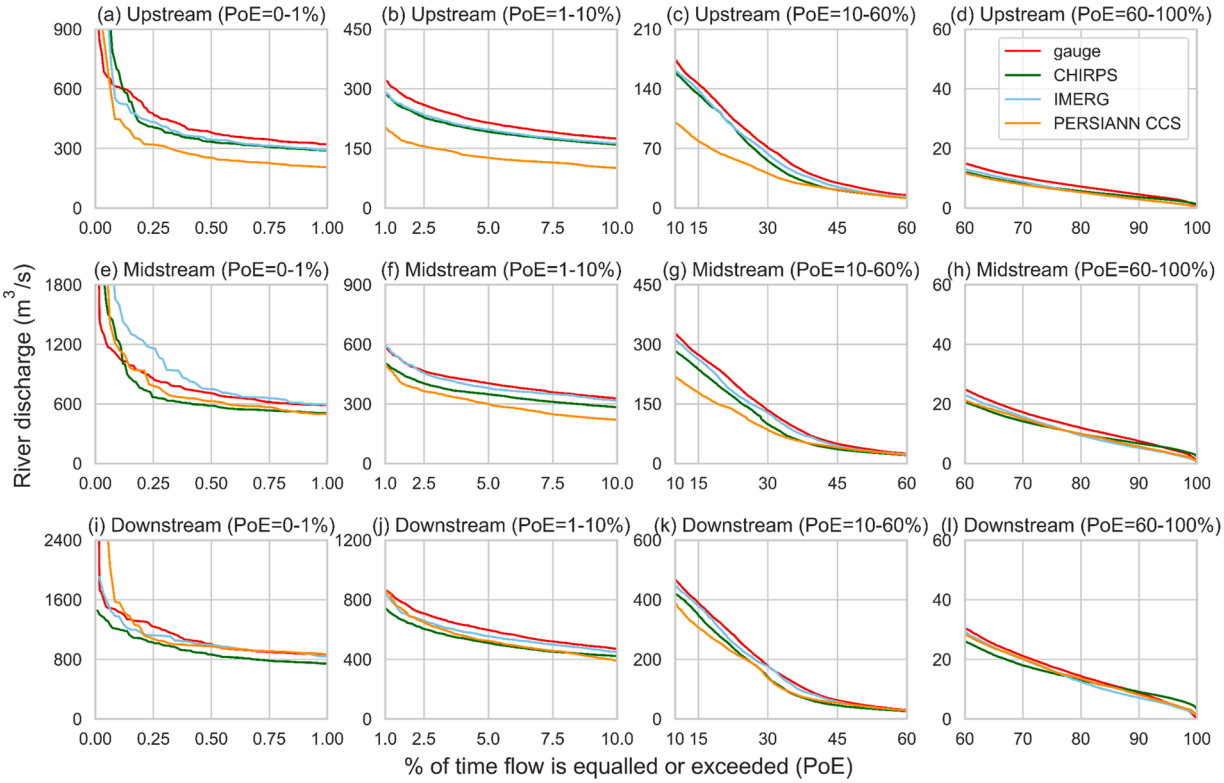

Fig. 9. Flow duration curve showing probability of exceedence (PoE) based on simulated river discharge using gauge data (1981 – 2015) and different bias-corrected SPEs (CHIRPS: 1981-2015, IMERG: 2000-2015, and PERSIANN-CCS: 2003-2015) at three hydrologic gauge stations (upstream a-d, midstream e-h, and downstream i-l) in West Rapti River basin. First, second, third and fourth columns from left represent PoE ranging 0-1% (extremely high flow), 1-10 % (high flow), 10 – 60 % (average flow), and 60-100 % (low flow) respectively.

(calibration and validation periods), and ii) different SPEs in raw and corrected forms at three stations in upstream, midstream, and downstream of the study area. The figure well summarizes the improvement in model performance based on all three indices (NSE, R^2 and PBIAS values) after the implementation of bias-correction. Improvement for IMERG and CHIRPS was negligible compared to PERSIANN-CCS because the level of bias-correction was substantial for PERSIANN-CCS. NSE improved from ~ 0.15 to ~ 0.40, PBIAS improved from ~ -60 % to ~ -20 %, and R^2 improved from ~ 0.4 to ~ 0.45 for PERSIANN-CCS.

Fig. 9 illustrates a similar disaggregated FDCs as in Fig. 5 but for the simulations based on bias-corrected SPEs. The corrected SPEs displayed nearly congruous pattern at all the four different ranges of PoEs (extremely high, high, average, and low). However, there exists some noticeable discrepancies. PERSIANN-CCS, even after the implementation of bias-correction, showed noticeable underestimation in extremely high (PoE = 0–1%), and high (PoE = 1–10%) zones, and slight underestimation in average (PoE = 10–60 %) zone of PoEs at the upstream station. The results indicate that spatially uniform correction factor throughout the study area might not replicate a realistic bias reduction at upstream region of the study area. One of the possible reasons is elevation heterogeneity since the upstream region is a hilly topography with a maximum elevation of 3618 m asl whereas lower region is almost flat. We might need to consider an elevation dependencies (Karki et al., 2016) during the computation of bias-correction. The graphical as well as statistical analyses clearly depict the potential of using SPEs for watershed scale rainfall-runoff analysis. We believe, SPEs could be used in data-scarce basins or to fill the data gap in gauge data for an effective water resource planning and management. Hereinafter, SPEs simply means corrected SPEs. Our next analysis involved the estimation of the precipitation elasticity of the basin using both SPEs and gauge data.

3.4. Precipitation elasticity

Fig. 10 shows the inter-annual variation of precipitation elasticity for gauge and SPEs at three stations in upstream, midstream, and downstream of the study area. The precipitation elasticity ranged from 1.3 to 1.6 in upstream and midstream (meaning upper WRR basin) whereas it ranged from 1.4 to 1.7 in downstream (meaning lower WRR basin). IMERG showed slightly greater values of precipitation elasticity for most of the years. In general, PERSIANN-CCS showed slightly lower values of precipitation elasticity compared to gauge-based. CHIRPS showed almost similar values of precipitation elasticity compared to gauge-based at downstream station but slightly smaller values at upstream and midstream stations. We found an average tendency of % change in river discharge is 1.5 times the % change in precipitation. For a simulation-based assessment, precipitation elasticity could be combined with other climatic

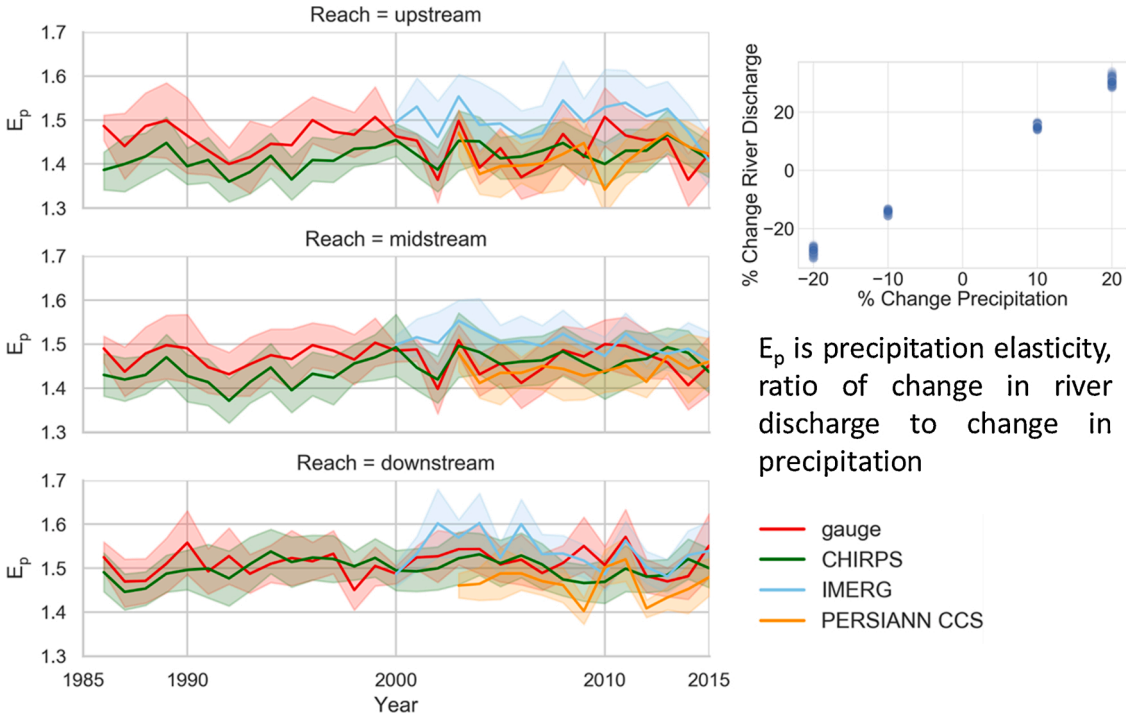

Fig. 10. Inter annual variation of precipitation elasticity (ε_p) based on simulation by scaling precipitation (gauge and different satellite-based precipitation estimates (SPEs)). Scaling of precipitation was done by -20 %, -10 %, +10 % and +20 %.

Table 5
Precipitation elasticity (ε_p) based on simulation by scaling precipitation (gauge and different satellite-based precipitation estimates (SPEs)) and non-parametric estimator (ε_p^{NP}) for observed and simulated data sets. Scaling of precipitation was done by -20 %, -10 %, +10 % and +20 % for gauge, and different SPEs. Non-parametric estimator of precipitation elasticity for simulated dataset was carried out for un-scaled precipitation for gauge, and different SPEs.

	Upstream	Midstream	Downstream	Data source	Remarks
ε_p	1.4 (1.3–1.6)	1.5 (1.3–1.6)	1.5 (1.4–1.7)	scaling gauge precipitation	
ε_p^{NP}	1.9	1.7	1.7	Non-parametric (gauge-based simulation)	
ε_p	1.4 (1.3–1.5)	1.4 (1.3–1.6)	1.5 (1.4–1.6)	scaling CHIRPS precipitation	
ε_p^{NP}	1.5	1.6	1.6	Non-parametric (CHIRPS-based simulation)	SWAT simulation
ε_p	1.5 (1.3–1.6)	1.5 (1.4–1.6)	1.5 (1.4–1.7)	scaling IMERG precipitation	
ε_p^{NP}	1.9	1.8	1.9	Non-parametric (IMERG-based simulation)	
ε_p	1.4 (1.3–1.5)	1.4 (1.3–1.5)	1.5 (1.4–1.6)	scaling PERSIANN-CCS precipitation	
ε_p^{NP}	1.5	1.4	1.4	Non-parametric (PERSIANN-CCS-based simulation)	
ε_p^{NP}	2.0	1.7	1.6	Non-parametric based on observed data	Observed

variables elasticity including potential evapotranspiration, temperature or others (Chiew, 2006) for an assessment of combined climate variables elasticity.

A non-parametric estimator showed the larger value of precipitation elasticity compared to that of simulation based on scaling the precipitation. Table 5 shows a detail of precipitation elasticity computed using both methods (simulated fed with scaled precipitation and non-parametric estimator) from different data sources. Based on gauge-based simulation and observed data, non-parametric precipitation elasticity was found to be ~2 for the upstream station and ~1.7 for midstream and downstream stations. IMERG-based simulation showed that nearly congruous value of non-parametric precipitation elasticity wrt gauge-based simulation. And remaining two SPEs showed slight lower values. In general, by implementing different techniques, we found the precipitation elasticity of the basin is ~1.5.

The relationship between precipitation elasticity and various catchment characteristics, based on the soils, vegetation and land use data sets are crucial for planning of water resources and water-induced disasters. In addition, practitioners and water resource managers are concerned about an anticipated change of precipitation elasticity under climate change and future land use. Our study, as the first kind of such study in Nepal, provides an understanding of precipitation elasticity of the study area using physically-based hydrologic model. We believe, similar studies in other watersheds could provide a broader vision of catchment response under changing climate variables. And finally, our study supports the application of selected SPEs for hydrologic modelling in similar regions

of the country.

4. Conclusion and outlook

This study firstly evaluated the performance of three selected SPEs. Both the detection-based and magnitude-based evaluation indices showed that the IMERG was superior and in contrast PERSIANN-CCS showed a significant underestimation. However, all SPEs showed significant false alarms. The FAR values ranged from ~0.4 to ~0.8 for CHIRPS and PERSIANN-CCS and from ~0.3 to ~0.8 for IMERG. Importantly, the tendency of intra-annual variability is well captured by all three SPEs indicating the applicability of the SPEs. However, a proper systematic biases should be evaluated to reduce the contaminated biases. After the implementation of bias-correction of those SPEs at different levels, all products revealed improved results and the simulated river discharges were nearly congruous to observed data.

In general, intra-annual variability of precipitation and river discharge was well represented by all three SPEs. We found IMERG to be superior among selected SPEs. The annual correction factor for CHIRPS and IMERG was found to be 1.1 while it was 1.9 for PERSIANN-CCS. Selected SPEs could be used in data-scarce basins or to fill the data gap in gauge data for an effective water resource planning and management.

For the analyses of different zones of river discharges based on PoEs, this study categorized the flows into four ranges i) extremely high (PoE = 0–1%), ii) high (PoE = 1–10%), iii) average (PoE = 10–60 %), and iv) low (PoE = 60–100%). For the extremely high flow, the simulated discharge revealed significant underestimation indicating the limitations of the SWAT model to effectively mimic the timing, intensity, and magnitude of peak flood (PoE $\leq$1%).

The current study evaluated precipitation elasticity by two methods: i) a non-parametric estimator and ii) by scaling the gauge precipitation and SPEs data in both positive and negative directions (ranging from -20 % to +20 %). A non-parametric estimator showed the larger value of precipitation elasticity compared to that of simulation-based on scaling the precipitation. In general, by implementing different techniques, we found the precipitation elasticity of the basin is ~1.5.

CRediT authorship contribution statement

Rocky Talchabhadel: Conceptualization, Data curation, Methodology, Software, Investigation, Writing - original draft, Writing - review & editing. **Anil Aryal:** Conceptualization, Methodology, Writing - review & editing. **Kenji Kawaike:** Conceptualization, Supervision, Writing - review & editing. **Kazuki Yamanoi:** Conceptualization, Supervision, Writing - review & editing. **Hajime Nakagawa:** Conceptualization, Supervision, Writing - review & editing. **Binod Bhatta:** Conceptualization, Writing - review & editing. **Saroj Karki:** Conceptualization, Methodology, Writing - review & editing. **Bhesh Raj Thapa:** Conceptualization, Methodology, Writing - review & editing.

Declaration of Competing Interest

The authors declare that they have no known competing financial interests or personal relationships that could have appeared to influence the work reported in this paper.

Acknowledgements

This work was supported by the Japan Society for the Promotion of Science Postdoctoral Fellowship Program (grant in aid P19052). We would like to thank the Department of Hydrology and Meteorology, and the Department of Survey, Government of Nepal for sharing hydro-meteorological and survey data respectively.

Appendix A. Supplementary data

Supplementary material related to this article can be found, in the online version, at doi:https://doi.org/10.1016/j.ejrh.2020.100768.

References

Abbaspour, K.C., Johnson, C.A., van Genuchten, M.T., 2004. Estimating Uncertain flow and transport parameters using a sequential uncertainty fitting procedure. Vadose Zone J. 3, 1340–1352. https://doi.org/10.2136/vzj2004.1340.

Abbaspour, K.C., Faramarzi, M., Ghasemi, S.S., Yang, H., 2009. Assessing the impact of climate change on water resources in Iran. Water Resour. Res. 45, 1–16. https://doi.org/10.1029/2008WR007615.

Ahn, S., Abudu, S., Sheng, Z., Mirchi, A., 2018. Hydrologic impacts of drought-adaptive agricultural water management in a semi-arid river basin: case of Rincon Valley, New Mexico. Agric. Water Manag. 209, 206–218. https://doi.org/10.1016/j.agwat.2018.07.040.

Alazzy, A.A., Lü, H., Chen, R., Ali, A.B., Zhu, Y., Su, J., 2017. Evaluation of satellite precipitation products and their potential influence on hydrological modeling over the Ganzi River Basin of the Tibetan Plateau. Adv. Meteorol. 2017 https://doi.org/10.1155/2017/3695285.

Arnold, J.G., Kiniry, J.R., Srinivasan, R., Williams, J.R., Haney, E.B., Neitsch, S.L., 2012a. Input/Output Documentation Soil & Water Assessment Tool.

Arnold, J.G., Moriasi, D.N., Gassman, P.W., Abbaspour, K.C., White, M.J., Srinivasan, R., Santhi, C., Harmel, R.D., van Griensven, A., van Liew, M.W., Kannan, N., Jha, M.K., 2012b. SWAT: model use, calibration, and validation. Trans. ASABE 55, 1509–1522. https://doi.org/10.13031/2013.42259.

Aryal, A., Shrestha, S., Babel, M.S., 2019. Quantifying the sources of uncertainty in an ensemble of hydrological climate-impact projections. Theor. Appl. Climatol. 135, 193–209. https://doi.org/10.1007/s00704-017-2359-3.

Ashouri, H., Hsu, K.L., Sorooshian, S., Braithwaite, D.K., Knapp, K.R., Cecil, L.D., Nelson, B.R., Prat, O.P., 2015. PERSIANN-CDR: daily precipitation climate data record from multisatellite observations for hydrological and climate studies. Bull. Am. Meteorol. Soc. 96, 69–83. https://doi.org/10.1175/BAMS-D-13-00068.1.

Beck, H.E., van Dijk, A.I.J.M., Levizzani, V., Schellekens, J., Miralles, D.G., Martens, B., de Roo, A., 2017. MSWEP: 3-hourly 0.25° global gridded precipitation (1979–2015) by merging gauge, satellite, and reanalysis data. Hydrol. Earth Syst. Sci. 21, 589–615. https://doi.org/10.5194/hess-21-589-2017.

Behrangi, A., Khakbaz, B., Jaw, T.C., AghaKouchak, A., Hsu, K., Sorooshian, S., 2011. Hydrologic evaluation of satellite precipitation products over a mid-size basin. J. Hydrol. 397, 225–237. https://doi.org/10.1016/j.jhydrol.2010.11.043.

Berg, P., Norin, L., Olsson, J., 2016. Creation of a high resolution precipitation data set by merging gridded gauge data and radar observations for Sweden. J. Hydrol. 541, 6–13. https://doi.org/10.1016/j.jhydrol.2015.11.031.

Bharati, L., Gurung, P., Maharjan, L., Bhattarai, U., 2016. Past and future variability in the hydrological regime of the Koshi Basin, Nepal. Hydrol. Sci. J. 61, 79–93. https://doi.org/10.1080/02626667.2014.952639.

Bhatta, B., Shrestha, S., Shrestha, P.K., Talchabhadel, R., 2019. Evaluation and application of a SWAT model to assess the climate change impact on the hydrology of the Himalayan River Basin. CATENA 181, 104082. https://doi.org/10.1016/j.catena.2019.104082.

Bhatta, B., Shrestha, S., Shrestha, P.K., Talchabhadel, R., 2020. Modelling the impact of past and future climate scenarios on streamflow in a highly mountainous watershed: a case study in the West Seti River Basin, Nepal. Sci. Total Environ. 740, 140156 https://doi.org/10.1016/j.scitotenv.2020.140156.

Brocca, L., Filippucci, P., Hahn, S., Ciabatta, L., Massari, C., Camici, S., Schüller, L., Bojkov, B., Wagner, W., 2019. SM2RAIN–ASCAT (2007–2018): global daily satellite rainfall data from ASCAT soil moisture observations. Earth Syst. Sci. Data 11, 1583–1601. https://doi.org/10.5194/essd-11-1583-2019.

Bui, H.T., Ishidaira, H., Shaowei, N., 2019. Evaluation of the use of global satellite–gauge and satellite-only precipitation products in stream flow simulations. Appl. Water Sci. 9, 1–15. https://doi.org/10.1007/s13201-019-0931-y.

Chiew, F.H.S., 2006. Estimation of rainfall elasticity of streamflow in Australia. Hydrol. Sci. J. 51, 613–625. https://doi.org/10.1623/hysj.51.4.613.

Cole, S.J., Moore, R.J., 2008. Hydrological modelling using raingauge- and radar-based estimators of areal rainfall. J. Hydrol. 358, 159–181. https://doi.org/10.1016/j.jhydrol.2008.05.025.

Dahal, V., Shakya, N.M., Bhattarai, R., 2016. Estimating the impact of climate change on water availability in Bagmati Basin, Nepal. Environ. Process. 3, 1–17. https://doi.org/10.1007/s40710-016-0127-5.

Dembélé, M., Hrachowitz, M., Savenije, H.H.G., Mariéthoz, G., Schaefli, B., 2020. Improving the predictive skill of a distributed hydrological model by calibration on spatial patterns with multiple satellite data sets. Water Resour. Res. 56, 0–3. https://doi.org/10.1029/2019WR026085.

Dhami, B., Himanshu, S.K., Pandey, A., Gautam, A.K., 2018. Evaluation of the SWAT model for water balance study of a mountainous snowfed river basin of Nepal. Environ. Earth Sci. 77, 1–20. https://doi.org/10.1007/s12665-017-7210-8.

Dwarakish, G.S., Ganasri, B.P., 2015. Impact of land use change on hydrological systems: a review of current modeling approaches. Cogent Geosci. 1 https://doi.org/10.1080/23312041.2015.1115691.

Funk, C., Peterson, P., Landsfeld, M., Pedreros, D., Verdin, J., Shukla, S., Husak, G., Rowland, J., Harrison, L., Hoell, A., Michaelsen, J., 2015a. The climate hazards infrared precipitation with stations—a new environmental record for monitoring extremes. Sci. Data 2, 150066. https://doi.org/10.1038/sdata.2015.66.

Funk, C., Verdin, A., Michaelsen, J., Peterson, P., Pedreros, D., Husak, G., 2015b. A global satellite-assisted precipitation climatology. Earth Syst. Sci. Data 7, 275–287. https://doi.org/10.5194/essd-7-275-2015.

Huffman, G.J., Bolvin, D.T., Braithwaite, D., Hsu, K.-L., Joyce, R., Kidd, C., Nelkin, E.J., Sorooshian, S., Tan, J., Xie, P., 2019. Algorithm Theoretical Basis Document (ATBD) Version 06 NASA Global Precipitation Measurement (GPM) Integrated Multi-satellitE Retrievals for GPM (IMERG).

ICIMOD, 2013. Land Cover of Nepal 2010 [Data Set]. ICIMOD. https://doi.org/10.26066/rds.9224.

Johnston, R., Smakhtin, V., 2014. Hydrological modeling of large river basins: how much is enough? Water Resour. Manag. 28, 2695–2730. https://doi.org/10.1007/s11269-014-0637-8.

Karki, R., Talchabhadel, R., Aalto, J., Baidya, S.K., 2016. New climatic classification of Nepal. Theor. Appl. Climatol. 125, 799–808. https://doi.org/10.1007/s00704-015-1549-0.

Kidd, C., Becker, A., Huffman, G.J., Muller, C.L., Joe, P., Skofronick-Jackson, G., Kirschbaum, D.B., 2017. So, how much of the earth's surface is covered by rain gauges? Bull. Am. Meteorol. Soc. 98, 69–78. https://doi.org/10.1175/BAMS-D-14-00283.1.

King, K.W., Arnold, J.G., Bingner, R.L., 1999. Comparison of green-ampt and curve number methods on goodwin creek watershed using SWAT. Trans. ASAE 42, 919–926. https://doi.org/10.13031/2013.13272.

Krause, P., Boyle, D.P., Base, F., 2005. Comparison of different efficiency criteria for hydrological model assessment. Adv. Geosci. 5, 89–97.

Kumar, D., Gautam, A.K., Palmate, S.S., Pandey, A., Suryavanshi, S., Rathore, N., Sharma, N., 2017. Evaluation of TRMM multi-satellite precipitation analysis (TMPA) against terrestrial measurement over a humid sub-tropical basin, India. Theor. Appl. Climatol. 129, 783–799. https://doi.org/10.1007/s00704-016-1807-9.

Levizzani, V., Cattani, E., 2019. Satellite remote sensing of precipitation and the terrestrial water cycle in a changing climate. Remote Sens. 11 https://doi.org/10.3390/rs11192301.

Maggioni, V., Meyers, P.C., Robinson, M.D., 2016. A review of merged high-resolution satellite precipitation product accuracy during the Tropical Rainfall Measuring Mission (TRMM) era. J. Hydrometeorol. 17, 1101–1117. https://doi.org/10.1175/JHM-D-15-0190.1.

Maidment, R.I., Grimes, D., Black, E., Tarnavsky, E., Young, M., Greatrex, H., Allan, R.P., Stein, T., Nkonde, E., Senkunda, S., Alcántara, E.M.U., 2017. A new, long-term daily satellite-based rainfall dataset for operational monitoring in Africa. Sci. Data 4. https://doi.org/10.1038/sdata.2017.63.

Masaki, Y., Hanasaki, N., Biemans, H., Schmied, H.M., Tang, Q., Wada, Y., Gosling, S.N., Takahashi, K., Hijioka, Y., 2017. Intercomparison of global river discharge simulations focusing on dam operation - Multiple models analysis in two case-study river basins, Missouri-Mississippi and Green-Colorado. Environ. Res. Lett. 12 https://doi.org/10.1088/1748-9326/aa57a8.

Mishra, Y., Nakamura, T., Babel, M.S., Ninsawat, S., Ochi, S., 2018. Impact of climate change on water resources of the Bheri River Basin, Nepal. Water (Switzerland) 10, 1–21. https://doi.org/10.3390/w10020220.

Moriasi, D.N., Arnold, J.G., Van Liew, M.W., Bingner, R.L., Harmel, R.D., Veith, T.L., 2007. Model evaluation guidelines for systematic quantification of accuracy in watershed simulations. Trans. ASABE 50, 885–900. https://doi.org/10.13031/2013.23153.

Nash, J.E., Sutcliffe, J.V., 1970. River flow forecasting through conceptual models part I — a discussion of principles. J. Hydrol. 10, 282–290. https://doi.org/10.1016/0022-1694(70)90255-6.

Neitsch, S.L., Arnold, J.G., Kiniry, J.R., Williams, J.R., 2011. Soil & water assessment tool theoretical documentation version 2009. Texas Water Resour. Inst. 1–647.

Nguyen, P., Ombadi, M., Sorooshian, S., Hsu, K., AghaKouchak, A., Braithwaite, D., Ashouri, H., Thorstensen, A.R., 2018. The PERSIANN family of global satellite precipitation data: a review and evaluation of products. Hydrol. Earth Syst. Sci. 22, 5801–5816. https://doi.org/10.5194/hess-22-5801-2018.

Ning, S., Song, F., Udmale, P., Jin, J., Thapa, B.R., Ishidaira, H., 2017. Error analysis and evaluation of the latest GSMap and IMERG precipitation products over Eastern China. Adv. Meteorol. 2017, 1–16. https://doi.org/10.1155/2017/1803492.

OECD, 2008. Space Technologies and Climate Change. Space Technologies and Climate Change. https://doi.org/10.1787/9789264054196-en.

Olivera, F., Valenzuela, M., Srinivasan, R., Choi, J., Cho, H., Koka, S., Agrawal, A., 2006. ARCGIS-SWAT: a geodata model and GIS INTERFACE FOR SWAT. J. Am. Water Resour. Assoc. 42, 295–309. https://doi.org/10.1111/j.1752-1688.2006.tb03839.x.

Pandey, V.P., Dhaubanjar, S., Bharati, L., Thapa, B.R., 2019. Hydrological response of Chamelia watershed in Mahakali Basin to climate change. Sci. Total Environ. 650, 365–383. https://doi.org/10.1016/j.scitotenv.2018.09.053.

Pandey, V.P., Dhaubanjar, S., Bharati, L., Thapa, B.R., 2020a. Spatio-temporal distribution of water availability in Karnali-Mohana Basin, Western Nepal: hydrological model development using multi-site calibration approach (Part-A). J. Hydrol. Reg. Stud. 100690. https://doi.org/10.1016/j.ejrh.2020.100690.

Pandey, V.P., Shrestha, D., Adhikari, M., Shakya, S., 2020b. Streamflow alterations, attributions, and implications in extended east rapti watershed, central-southern Nepal. Sustainability 12, 3829. https://doi.org/10.3390/su12093829.
Qiu, J., Yang, Q., Zhang, X., Huang, M., Adam, J.C., Malek, K., 2019. Implications of water management representations for watershed hydrologic modeling in the Yakima River basin. Hydrol. Earth Syst. Sci. 23, 35–49. https://doi.org/10.5194/hess-23-35-2019.
Sanchez-Moreno, J.F., Mannaerts, C.M., Jetten, V., 2014. Influence of topography on rainfall variability in Santiago island, Cape Verde. Int. J. Climatol. 34, 1081–1097. https://doi.org/10.1002/joc.3747.
Sankarasubramanian, A., Vogel, R.M., Limbrunner, J.F., 2001. Climate elasticity of streamflow in the United States. Water Resour. Res. 37, 1771–1781. https://doi.org/10.1029/2000WR900330.
Schmalz, B., Strehmel, A., Song, S., Kuemmerlen, M., Cai, Q., Jähnig, S., Fohrer, N., 2012. Hydrological and hydraulic results of an integrated modelling approach in a mesoscale Chinese catchment. EGU Gen. Assem. Geophys. Res. Abstr. 14, 2810.
Siddique-E-Akbor, A.H.M., Hossain, F., Sikder, S., Shum, C.K., Tseng, S., Yi, Y., Turk, F.J., Limaye, A., 2014. Satellite precipitation data–Driven hydrological modeling for water resources management in the Ganges, Brahmaputra, and meghna basins. Earth Interact. 18, 1–25. https://doi.org/10.1175/ei-d-14-0017.1.
Singh, V.P., 2018. Hydrologic modeling: progress and future directions. Geosci. Lett. 5, 15. https://doi.org/10.1186/s40562-018-0113-z.
Sun, Q., Miao, C., Duan, Q., Ashouri, H., Sorooshian, S., Hsu, K.L., 2018. A review of global precipitation data sets: data sources, estimation, and intercomparisons. Rev. Geophys. 56, 79–107. https://doi.org/10.1002/2017RG000574.
Talchabhadel, R., Sharma, R., 2014. Real time data analysis of West Rapti River Basin of Nepal. J. Geosci. Environ. Prot. 02, 1–7. https://doi.org/10.4236/gep.2014.25001.
Talchabhadel, R., Karki, R., Thapa, B.R., Maharjan, M., Parajuli, B., 2018. Spatio-temporal variability of extreme precipitation in Nepal. Int. J. Climatol. 38, 4296–4313. https://doi.org/10.1002/joc.5669.
Talchabhadel, R., Aryal, A., Kawaike, K., Yamanoi, K., Nakagawa, H., 2020a. A comprehensive analysis of projected changes of extreme precipitation indices in West Rapti River basin, Nepal under changing climate. Int. J. Climatol., joc.6866 https://doi.org/10.1002/joc.6866.
Talchabhadel, R., Nakagawa, H., Kawaike, K., Prajapati, R., 2020b. Evaluating the rainfall erosivity (R-factor) from daily rainfall data: an application for assessing climate change impact on soil loss in Westrapti River basin, Nepal. Model. Earth Syst. Environ. https://doi.org/10.1007/s40808-020-00787-w.
Tang, Q., Gao, H., Lu, H., Lettenmaier, D.P., 2009. Remote sensing: hydrology. Prog. Phys. Geogr. 33, 490–509. https://doi.org/10.1177/0309133309346650.
Tarek, M., Brissette, F.P., Arsenault, R., 2020. Evaluation of the ERA5 reanalysis as a potential reference dataset for hydrological modelling over North America. Hydrol. Earth Syst. Sci. 24, 2527–2544. https://doi.org/10.5194/hess-24-2527-2020.
Thapa, B.R., Ishidaira, H., Bui, T.H., Shakya, N.M., 2016. Evaluation of water resources in mountainous region of Kathmandu Valley using high resolution satellite precipitation product. J. Japan Soc. Civ. Eng. Ser. G (Environmental Res. 72, I_27–I_33. https://doi.org/10.2208/jscejer.72.I_27.
Thapa, B.R., Ishidaira, H., Pandey, V.P., Shakya, N.M., 2017. A multi-model approach for analyzing water balance dynamics in Kathmandu Valley, Nepal. J. Hydrol. Reg. Stud. 9, 149–162. https://doi.org/10.1016/j.ejrh.2016.12.080.
Uddin, K., Shrestha, H.L., Murthy, M.S.R., Bajracharya, B., Shrestha, B., Gilani, H., Pradhan, S., Dangol, B., 2015. Development of 2010 national land cover database for the Nepal. J. Environ. Manage. 148, 82–90. https://doi.org/10.1016/j.jenvman.2014.07.047.
Vano, J.A., Das, T., Lettenmaier, D.P., 2012. Hydrologic sensitivities of Colorado River runoff to changes in precipitation and temperature. J. Hydrometeorol. 13, 932–949. https://doi.org/10.1175/JHM-D-11-069.1.
Wang, Y., Jiang, R., Xie, J., Zhao, Y., Yan, D., Yang, S., 2019. Soil and water assessment tool (SWAT) model: a systemic review. J. Coast. Res. 93, 22. https://doi.org/10.2112/SI93-004.1.
Wehbe, Y., Ghebreyesus, D., Temimi, M., Milewski, A., Al Mandous, A., 2017. Assessment of the consistency among global precipitation products over the United Arab Emirates. J. Hydrol. Reg. Stud. 12, 122–135. https://doi.org/10.1016/j.ejrh.2017.05.002.
Xue, L., Yang, F., Yang, C., Chen, X., Zhang, L., Chi, Y., Yang, G., 2017. Identification of potential impacts of climate change and anthropogenic activities on streamflow alterations in the Tarim River Basin, China. Sci. Rep. 7, 1–12. https://doi.org/10.1038/s41598-017-09215-z.
Yang, Y., Wang, G., Wang, L., Yu, J., Xu, Z., 2014. Evaluation of gridded precipitation data for driving SWAT model in area upstream of three gorges reservoir. PLoS One 9. https://doi.org/10.1371/journal.pone.0112725.
Zandler, H., Haag, I., Samimi, C., 2019. Evaluation needs and temporal performance differences of gridded precipitation products in peripheral mountain regions. Sci. Rep. 9, 1–15. https://doi.org/10.1038/s41598-019-51666-z.
Zhang, L., Nan, Z., Xu, Y., Li, S., 2016. Hydrological impacts of land use change and climate variability in the headwater region of the Heihe River Basin, northwest China. PLoS One 11, 1–25. https://doi.org/10.1371/journal.pone.0158394.